REFINED METALLICITY INDICES FOR M DWARFS USING THE SLoWPoKES CATALOG OF WIDE, LOW-MASS BINARIES

SAURAV DHITAL[1,2,7], ANDREW A. WEST[2,8], KEIVAN G. STASSUN[1,3,4], JOHN J. BOCHANSKI[5],
ANGELA P. MASSEY[2,6], AND FABIENNE A. BASTIEN[1]

[1] Department of Physics & Astronomy, Vanderbilt University, 6301 Stevenson Center, Nashville, TN 37235, USA; saurav.dhital@vanderbilt.edu
[2] Department of Astronomy, Boston University, 725 Commonwealth Avenue, Boston, MA 02215, USA
[3] Department of Physics, Fisk University, 1000 17th Avenue N., Nashville, TN 37208, USA
[4] MIT Kavli Institute for Astrophysics, 77 Massachusetts Avenue, Cambridge, MA 02139, USA
[5] Astronomy and Astrophysics Department, Pennsylvania State University, 525 Davey Laboratory, University Park, PA 16802, USA
[6] Lusher Charter School, 5624 Freret St., New Orleans, LA 70115, USA

ABSTRACT

We report the results from spectroscopic observations of 113 ultra-wide, low-mass binary systems, largely composed of M0–M3 dwarfs, from the SLoWPoKES catalog of common proper motion pairs identified in the Sloan Digital Sky Survey. Radial velocities of each binary member were used to confirm that they are comoving and, consequently, to further validate the high fidelity of the SLoWPoKES catalog. Ten stars appear to be spectroscopic binaries based on broad or split spectral features, supporting previous findings that wide binaries are likely to be hierarchical systems. We measured the Hα equivalent width of the stars in our sample and found that components of 81% of the observed pairs have similar Hα levels. The difference in Hα equivalent width among components with similar masses was smaller than the range of Hα variability for individual objects. We confirm that the Lépine et al. ζ-index traces iso-metallicity loci for most of our sample of M dwarfs. However, we find a small systematic bias in ζ, especially in the early-type M dwarfs. We use our sample to recalibrate the definition of ζ. While representing a small change in the definition, the new ζ is a significantly better predictor of iso-metallicity for the higher-mass M dwarfs.

Key words: binaries: spectroscopic – binaries: visual – brown dwarfs – stars: abundances – stars: kinematics and dynamics – stars: low-mass – stars: magnetic field

Online-only material: color figures, machine-readable and VO tables

1. INTRODUCTION

Low-mass stars, generally defined as the regime bracketed by the hydrogen-burning limit ($\sim 0.08\,M_\odot$) and the onset of molecular lines in the photosphere ($\sim 0.8\,M_\odot$), make up $\sim 70\%$ of the Milky Way's stars (Bochanski et al. 2010) and are, perhaps, the best tracers of the structure, dynamics, and evolutionary history of the Galaxy. However, their intrinsic faintness has historically limited the construction of large samples. In addition, the ubiquitous molecular features in their photospheres and the resulting incomplete line lists have restricted the accuracy and usefulness of theoretical atmospheric models. Large surveys, such as the Sloan Digital Sky Survey (SDSS; York et al. 2000) and the Two Micron All Sky Survey (2MASS; Skrutskie et al. 2006), have played a large role in advancing our understanding of low-mass stars. With a photometric catalog of more than 33 million (Bochanski et al. 2010) and a spectroscopic catalog of more than 70,000 (West et al. 2011) M dwarfs, SDSS has enabled studies of the spatial (Bochanski et al. 2010) and kinematic distributions (Bochanski et al. 2007b; Fuchs et al. 2009) in the Milky Way, the mass and luminosity functions (Covey et al. 2008; Bochanski et al. 2010), and magnetic activity (e.g., West et al. 2008, 2011;

Kruse et al. 2010; Kowalski et al. 2009; Hilton et al. 2010) of low-mass stars.

The metallicity of low-mass stars remains an elusive parameter to measure. Given the large number of M dwarfs in the Milky Way, an absolute metallicity scale tied to an easily observable spectral index would allow for the tracing of the formation history and the chemical evolution of the Galaxy (e.g., West et al. 2008), the dependence of the fundamental mass–radius relation on metallicity at the bottom of the main sequence (e.g., López-Morales 2007), and the relationship between metallicity and the presence of planets (e.g., Laws et al. 2003; Valenti & Fischer 2008). While spectral modeling has allowed for metallicity determinations and well-defined metallicity indices for warmer stars, such efforts in the late-K and M spectral type regimes (e.g., Hauschildt et al. 1999; Witte et al. 2011) have met with notable problems due to the onset of broad molecular lines at $\lesssim 4300$ K and due to incomplete molecular line lists. Some authors have tried to use photometric indices to infer the metallicity (Bonfils et al. 2005; Johnson & Apps 2009; Schlaufman & Laughlin 2010), but these techniques rely on trigonometric parallax measurements that are uncommon for M dwarfs.

Some useful spectral features that correlate with metallicity have been identified. In the near-infrared, Rojas-Ayala et al. (2010) developed a metallicity indicator based on the strength of the Na I doublet, the Ca I triplet, and a temperature-sensitive water index. This technique has so far only been calibrated over a limited range but delivers the greatest precision among current techniques. Meanwhile, much effort has gone into

---

optical spectra. As the TiO band in the optical spectrum becomes weaker with decreasing metallicity (Bessell 1982), the ratio of CaH and TiO molecular bands has been used to distinguish M dwarfs from M subdwarfs (Kirkpatrick et al. 1991; Reid et al. 1995; Gizis 1997; Lépine et al. 2003; Burgasser & Kirkpatrick 2006). Building on these studies, Lépine et al. (2007, hereafter LRS07) defined the metallicity-dependent quantity ζ using the Reid et al. (1995) CaH2, CaH3, and TiO5 molecular band heads; this allowed for the segregation of low-mass dwarfs into four classes: dwarfs (dMs), subdwarfs (sdMs), extreme subdwarfs (esdMs), and ultra subdwarfs (usdMs). These classes may also trace the Galactic populations to which these stars belong: dMs were formed in the thin disk, sdMs in the thick disk, and esdMs/usdMs in the halo. LRS07 calibrated the definition of ζ using the visual binary pairs known at the time, including four sdM and two esdM pairs. Woolf et al. (2009) mapped the ζ index to an absolute metallicity scale using dM binaries with F, G, or K dwarf primaries for which the absolute metallicity can be measured, but it suffers from significant scatter ($\sim$0.3 dex).

Wide binary (or multiple) systems are ideal, coeval laboratories to constrain and calibrate the observable properties of stars as the components were presumably formed at the same time and from the same primordial material but have evolved independently. In Dhital et al. (2010, hereafter Paper I), we identified the Sloan Low-mass Wide Pairs of Kinematically Equivalent Stars (SLoWPoKES) catalog consisting of 1342 ultrawide, low-mass common proper motion (CPM) binary systems from the SDSS Data Release 7 (DR7; Abazajian et al. 2009) by matching angular separations, photometric distances, and proper motions. The binary systems in the catalog have at least one low-mass (spectral subtype K5 or later) component, projected physical separations of $\sim10^3$–10^5 AU, and distances of $\sim$50–800 pc. While most SLoWPoKES pairs are disk dwarfs, 70 low-metallicity sdM and 21 white dwarf–dM pairs were identified based on their reduced proper motions. A Galactic model—based on empirical constraints on the stellar number density (Bochanski et al. 2010; Jurić et al. 2008) and velocity (Bochanski et al. 2007a) distributions in the Milky Way—was used to assess the probability that the candidates were a chance alignment of random stars; only pairs with such probabilities $\leqslant$5% were published in the SLoWPoKES catalog. The overall fidelity of the catalog is expected to be $\sim$98%. Hence, the SLoWPoKES catalog is a very clean and diverse source of CPM binary systems to be used in follow-up studies. As the SLoWPoKES catalog spans a wide range in mass and a smaller, but still considerable, range in metallicity, it is an ideal sample to constrain the ζ index and to eventually map it to an absolute metallicity space.

Magnetic activity has been shown to decline with age, with activity lifetimes of $\sim$1–2 Gyr for M0–M3 and $\sim$7–8 Gyr for M5–M7 dwarfs (West et al. 2006, 2008, 2011). This monotonic decline of activity with age is a signature of stellar spin-down and suggestive of a gyrochronology-like age–rotation–activity relationship in M dwarfs (Skumanich 1972; Barnes 2003, 2007; Delorme et al. 2010). Leveraging the coevality of components of the SLoWPoKES pairs is a good way of testing this relationship.

We have carried out a spectroscopic follow-up study of 113 CPM pairs from the SLoWPoKES catalog. Section 2 details our observations and the data reduction procedures. In Section 3 we use our radial velocities to assess the fidelity of the observed SLoWPoKES pairs, use them to redefine the LRS07 ζ index, and examine the magnetic activity properties of the SLoWPoKES pairs. The conclusions are presented in Section 4.

Table 1
Radial Velocity Standards from Delfosse et al. (1998)

Name	Spectral Type	V_r (km s^{-1})
GJ 1057	M4	27
GJ 1093a	M4	−30
GJ 1111	M8	9
GJ 1156	M5	4
Gl 70	M2	−26
Gl 105b	M3	26
Gl 109	M2	30
G 165−08	M4	8
Gl 205	M0	8
Gl 251	M2	22
Gl 338	M0	11
Gl 380	K5	−26
Gl 411	M2	−85
Gl 412B	M5	68
Gl 450	M1	0
Gl 514	M0	14
Gl 581	M2	−10
Gl 623	M2	−27
Gl 625	M1	−13
LHS 1805	M4	1
LHS 2520	M3	80
LHS 1885	M4	16

2. OBSERVATIONS AND DATA REDUCTION

The spectroscopic targets were selected from the SLoW-PoKES catalog based on their brightnesses, colors, and inferred mass ratios. Both components were required to be brighter than $r \sim 17$ so as to obtain the desired signal-to-noise ratio (S/N) within a reasonable integration time. Efforts were made to obtain (1) an even distribution in $r-z$ space for both the primary and secondary components and (2) a roughly equal number of equal-mass (within 5% of each other) and unequal-mass ($\gtrsim$5% of each other) systems. We estimated masses from the $r-z$ colors based on Kraus & Hillenbrand (2007).

Observations were carried out with the GoldCam spectrograph on the KPNO 2.1 m telescope on two separate observing runs on 2009 January 11–16 UT and 2010 March 26–31 UT. For both runs, the 36 grating (1200 lines mm^{-1}) in the first order, blazed at 7500 Å, along with the OG 550 order-blocking filter were used, resulting in a wavelength coverage of $\sim$6200–8200 Å with a dispersion of 0.62 Å pixel^{-1}. A slit width of 2″ was used to maximize the number of photons collected, yielding an effective resolution of 1.8 Å and a resolving power of 3500. Both components of a binary were observed at the same time by rotating the slit to align with the position angle of the binary. While the rotation had to be done manually and required $\sim$10 minutes of overhead time, it was more efficient than observing each component separately.

Each night quartz flats and biases were taken before the targets were observed; when the first half of the night was lost owing to weather, the flats and biases were taken in the morning. For wavelength calibration, HeNeAr comparison arcs, along with the BG 38 order-blocking filter, were generally taken after each target or when the CCD orientation was rotated. A suite of radial velocity standards from Delfosse et al. (1998) were observed and are listed in Table 1, which we used to assess our radial velocity precision (see below). Similarly, a flux standard—HZ 44, a bright sdO star—was observed each night during the second run. Both observing runs were conducted in bright time, often
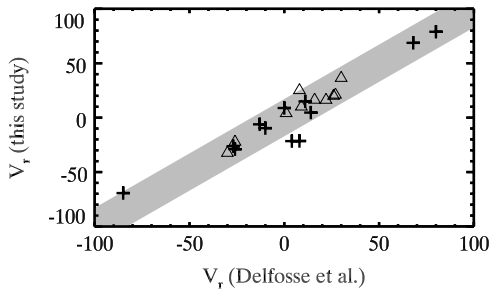
Figure 1. Comparison of the radial velocities for the standard stars from the 2009 (triangles) and 2010 (pluses) observation runs selected from Delfosse et al. (1998) shows no systematic trends. The m.a.d. of the difference between Delfosse et al. (1998) and the measured V_r was 5.7 km s^{-1}; we adopt this value as the error in our radial velocity measurements. The 3 m.a.d. regime is shaded in gray.

during non-photometric seeing. A combination of clouds and high winds caused the loss of 3–4 nights between the two runs.

All spectra were bias subtracted, flat fielded, extracted, co-added, wavelength calibrated, and flux calibrated[9] using standard IRAF[10] procedures, following the prescription detailed in Massey et al. (1992). Eighteen pairs where one of the components (usually the fainter secondary) was not well calibrated or had low S/N were removed from the sample. The stars were then manually spectral typed with the HAMMER pipeline (Covey et al. 2007); the error in the process is expected to be smaller than one sub-type, as discussed by West et al. (2011).

The radial velocities (V_r) of the stars were measured by cross-correlating the spectra using IDL routine XCORL.PRO (Mohanty & Basri 2003; West & Basri 2009) with the appropriate spectral type templates from Bochanski et al. (2007b), which are in the heliocentric rest frame. The cross-correlation was performed in the wavelength range of 6600–7550 Å. Since templates are only available for M0–L0 dwarfs, M0 templates were used for K7 dwarfs. However, as each spectral type spans a range in mass and temperature, the spectral features in stars of the same sub-type can differ significantly. This is probably the largest source of error in measuring V_r with the cross-correlation techniques. However, cross-correlation with templates typically yields V_r with $\lesssim 10$ km s^{-1} precision for SDSS spectra (Bochanski et al.

---

[9] As flux calibrations were not taken for the first run, we used a subset of radial velocity standards, which had absolute flux measurements as part of the Palomar–Michigan State Survey (Reid et al. 1995), as flux standards.
[10] IRAF is distributed by the National Optical Astronomy Observatory, which is operated by the Association of Universities for Research in Astronomy (AURA) under cooperative agreement with the National Science Foundation.
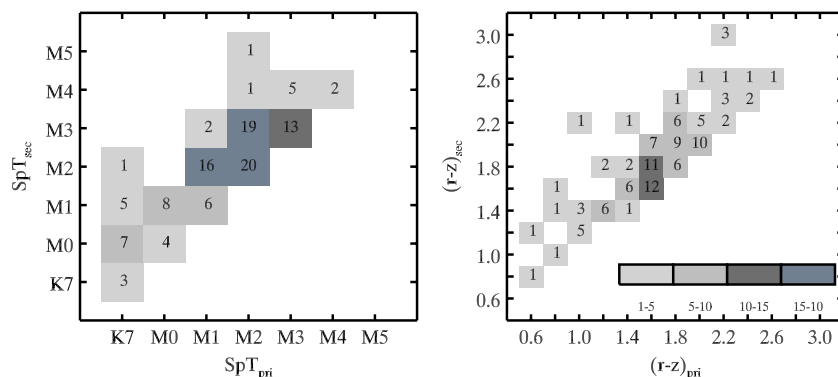
2007a). Other sources of error include difference in resolution between the template and object spectra and the accuracy of wavelength calibration, which was $\lesssim 0.04$ Å pixel^{-1} rms (1.4 km s^{-1}) for all but a few of the objects.

To assess the errors in our radial velocities, we cross-correlated the observed radial velocity standards (Delfosse et al. 1998) with appropriate templates from Bochanski et al. (2007b). Figure 1 shows the comparison between our measured values and the Delfosse et al. (1998) values, which were measured from high-resolution spectra. Apart from three outliers from the 2010 seasons, our values compare well with Delfosse et al. (1998). The median absolute deviation (m.a.d.) of the difference was 5.7 km s^{-1}; we adopt 6 km s^{-1} as the typical error in our measurement of V_r.

The spectra were then corrected for the measured radial velocities to be in the heliocentric rest frame and fed back into the HAMMER pipeline to measure the equivalent width of Hα; the molecular band strengths of CaH2, CaH3, and TiO features; and the S/N of the spectra, which was measured in the region spanning 6500–6550 Å.

3. RESULTS

Figure 2 shows the spectral type and $r - z$ color distributions of the primary and the secondary components of the 113 SLoWPoKES pairs that were observed (Table 2); the number of pairs in each bin is also shown. The observed sample, excluding pairs that were rejected for low S/N or other reasons, spans the K7–M4 spectral types ($r - z = 0.66$–2.52) for the primary and K7–M5 ($r - z = 0.77$–3.08) for the secondary. Even though our observed sample was limited to $r \sim 17$ and, thus, a dearth of late-type M dwarfs was to be expected, there are nonetheless 11 pairs with at least one component later than M4 and only 2 pairs with both components later than M4.

3.1. Spectroscopic Binaries

As discussed in Section 2, the radial velocities were measured by cross-correlating the program spectra with the appropriate SDSS template spectra (Bochanski et al. 2007b). The cross-correlation function (CCF) is used to determine the best match between the templates and program spectra. Presence of multiple turning points in the CCF, as well as unusual broadening of the spectrum, can indicate the presence of a spectroscopic binary (SB; Matijevič et al. 2010). While such a detection is unambiguous only in high-resolution spectra, we found possible evidence of SBs in our low-resolution spectra. Alternatively, the

Figure 2. Distribution of measured spectral types and $r - z$ colors for both the primary and secondary components of the 113 SLoWPoKES pairs observed in our KPNO run. The spectral types are shown in one subtype bin while the colors are in 0.2 mag bins. The background colors indicated the density in each bin, with the individual numbers printed as well. By definition, the primary always has an earlier spectral type and a bluer color than the secondary.
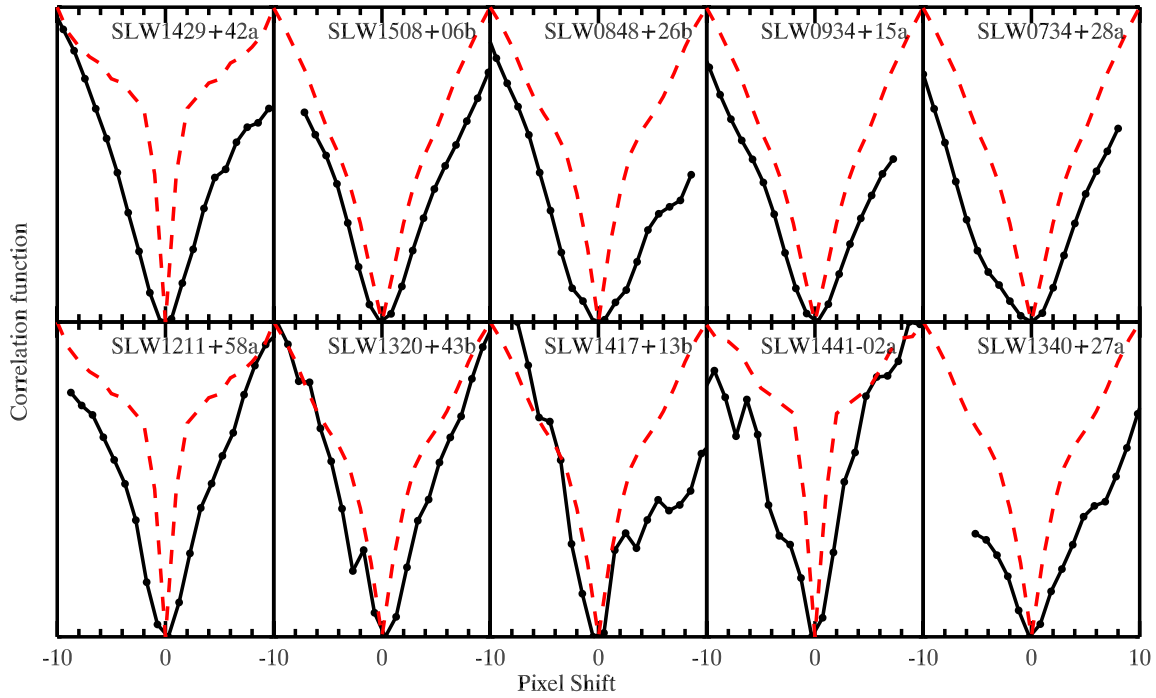
Figure 3. Broad CCFs (solid lines) and/or split spectral features indicate the presence of a tight companion in 10 of the observed systems. For reference, the autocorrelation function of our radial velocity standards is also shown (dashed lines). High-resolution spectra are needed to confirm the SBs. All spectra were corrected to the heliocentric rest frame.

(A color version of this figure is available in the online journal.)

Table 2
Properties of Observed SLoWPoKES Binaries

ID	Right Ascension		Declination		Distance		μ_α		μ_δ		V_r	
	A	B	A	B	A	B	A	B	A	B	A	B
SLW J2000	(hh mm ss.s)		(dd mm ss.ss)		(pc)		(mas yr^{-1})		(mas yr^{-1})		(km s^{-1})	
1512+20	15 12 22.52	15 12 25.41	+20 28 20.6	+20 28 12.3	63	58	−49	−48	4	7	−84.8	−77.8
0831+36	08 31 23.12	08 31 23.16	+36 54 41.8	+36 54 17.2	70	83	49	46	−54	−57	−30.8	−25.9
0741+19	07 41 55.34	07 41 57.06	+19 55 45.8	+19 55 33.3	66	78	−36	−35	−27	−27	31.2	47.8
0957+37	09 57 57.18	09 57 55.63	+37 56 02.4	+37 55 52.8	87	75	−23	−23	−60	−59	−23.6	−31.2
1120+20	11 20 03.38	11 20 05.26	+20 46 53.2	+20 46 54.9	96	101	−37	−41	−2	0	−7.6	−40.6
0858+09	08 58 57.80	08 58 54.73	+09 36 59.1	+09 37 23.7	65	63	−111	−107	6	6	23.5	32.7
1527+49	15 27 52.04	15 27 50.57	+49 08 54.2	+49 09 47.4	70	65	−60	−63	50	53	−89.7	−90.2
0734+28	07 34 50.75	07 34 49.23	+28 17 39.7	+28 18 15.8	62	75	−27	−29	−28	−29	−2.3	−36.7
1318+47	13 18 15.49	13 18 15.00	+47 30 29.4	+47 31 33.7	47	47	−104	−103	33	35	−60.1	−71.6
1508+06	15 08 44.07	15 08 43.72	+06 46 25.9	+06 46 35.5	110	108	−42	−44	0	0	−80.4	−51.3

ID	r		$r-z$		Spectral Type		EW(Hα)		CaH2		CaH3		TiO5	
	A	B	A	B	A	B	A	B	A	B	A	B	A	B
SLW J2000	(mag)						(Å)							
1512+20	15.01	16.87	2.02	2.56	M3	M4	−0.18	0.00	0.45	0.36	0.72	0.63	0.44	0.34
0831+36	16.13	16.51	2.12	2.36	M3	M4	2.36	7.93	0.42	0.38	0.69	0.62	0.43	0.37
0741+19	16.29	16.67	2.22	2.46	M3	M4	3.06	7.18	0.43	0.41	0.69	0.67	0.42	0.38
0957+37	17.28	17.34	2.45	2.57	M3	M4	4.11	7.16	0.39	0.39	0.65	0.64	0.38	0.34
1120+20	16.62	17.09	2.13	2.32	M3	M3	7.16	0.99	0.46	0.44	0.72	0.70	0.45	0.45
0858+09	15.58	15.76	2.12	2.20	M3	M3	5.12	2.57	0.42	0.42	0.65	0.67	0.39	0.43
1527+49	16.00	17.01	2.19	2.57	M3	M4	4.83	1.08	0.32	0.41	0.59	0.68	0.31	0.41
0734+28	14.40	14.78	1.65	1.90	M2	M2	4.64	0.00	0.46	0.53	0.69	0.76	0.49	0.55
1318+47	15.19	17.40	2.20	2.95	M2	M5	1.95	3.94	0.41	0.33	0.68	0.62	0.42	0.27
1508+06	15.66	17.04	1.78	2.23	M2	M2	3.53	0.64	0.42	0.49	0.67	0.75	0.43	0.52

(This table is available in its entirety in machine-readable and Virtual Observatory (VO) forms in the online journal. A portion is shown here for guidance regarding its form and content.)

wide CCF could correspond to fast rotators, although our $v \sin i$ resolution of 35 km s^{-1} means they would have to be rotating at very high speeds. Figure 3 shows the CCF for the 10 SB

candidates (Table 3). All 10 candidates have a relatively high S/N, so the CCF is not a product of noisy spectral features. For comparison, the CCF for the radial velocity standards, which are
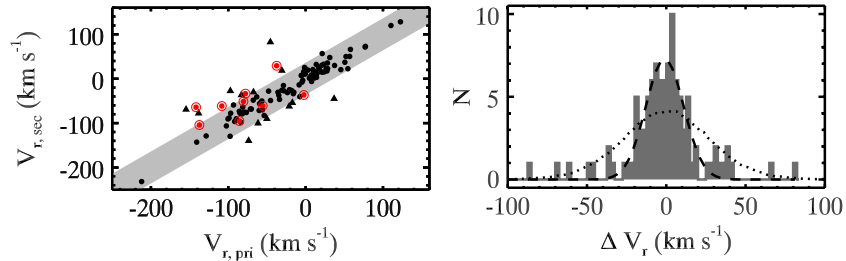
Figure 4. Left: the radial velocity of the primary and the secondary components: the pairs with $\Delta V_r > 3\sigma$ are shown as triangles while the candidate SBs, shown as red concentric circles, have larger ΔV_r. Right: the distribution of difference in radial velocities between components of SLoWPoKES pairs observed in this program, with the Gaussian fit shown by dashed lines. Eighty-five percent of the sample has $\Delta V_r \leqslant 3\sigma$. All pairs with $\Delta V_r > 50$ km s^{-1} have relatively low S/N. The expected intrinsic scatter in ΔV_r for two unassociated stars in the same three-dimensional position in the Galaxy and that have matching proper motions, as calculated using the Galactic model from Paper I, is shown with dotted lines; it is a much larger dispersion as compared with our observed sample of CPM pairs.

(A color version of this figure is available in the online journal.)

Table 3
Candidate Spectroscopic Binaries

Name	Spectral Type	Note
SLW 1211+58a	M0	. . .
SLW 1320+43b	M1	Wide CCF
SLW 1417+13b	M1	Wide CCF
SLW 1441-02a	K7	. . .
SLW 1340+27a	M1	Wide lines; wide CCF
SLW 1429+42a	M0	Double peak
SLW 1508+06b	M2	Wide CCF
SLW 0848+26b	M1	Wide CCF
SLW 0934+15a	M2	Line splitting; double peak
SLW 0734+28a	M	Line splitting, wide CCF

presumably single stars, of the corresponding spectral types are shown in red, dashed lines. High-resolution spectra are required to confirm these SBs.

Previous studies have found that components of wide binaries are more likely to have a companion as compared with single field stars. This enhanced binarity has been ascribed to the ease of transfer of angular momentum that facilitates the formation of close pairs (Tokovinin 1997; Bate et al. 2002; Burgasser et al. 2005; Connelley et al. 2009) and/or the stability of wide pairs in the field (Law et al. 2010). Among very low mass wide binaries, the frequency of tight companions is $50\% \pm 11\%$ (Faherty et al. 2010). In a sample of nearby SLoWPoKES pairs, Law et al. (2010) found that the bias-corrected higher-order multiplicity was $45^{+18}_{-16}\%$. While only 10 of the 113 pairs (8.8%) in this study have been identified as hierarchical, we were probing different kinds of hierarchical systems than those found by Law et al. (2010). Here we probed the extremely close pairs (SBs), whereas Law et al. (2010) probed systems with separations larger than 8–10 AU. In fact, our results are consistent with the Law et al. (2010) findings but limited to the extremely close pairs.

3.2. Fidelity of SLoWPoKES Pairs

The observed pairs were identified in Paper I based on a matching of their position, distance, and proper motions. The third velocity component, V_r, can be used to test the fidelity of the observed pairs and, by extrapolation, of the SLoWPoKES catalog.

Figure 4 shows the radial velocities of the primary component against that of the secondary in the left panel and the distribution of their differences in the right panel. The identified candidate SBs are shown as concentric circles. Excluding the 10 candidate SBs, 90 of the remaining 103 pairs (i.e., 87.4%) have ΔV_r within 3σ of the mean; the 3σ region is shown in gray in the left panel.

Overall, the ΔV_r distribution is well fit by a Gaussian with $\mu = -0.97 \pm 0.80$ km s^{-1} and $\sigma = 12.04 \pm 0.80$ km s^{-1}, shown as the dashed line though there are more outliers than expected (see below). As $\sigma \approx 1.4826$ m.a.d. for large normally distributed populations, $\sigma_{\Delta V_r} (= \sqrt{2} \times \sigma_{V_r} = \sqrt{2} \times 1.4826 \times 5.7$ km s$^{-1} = 11.95$ km s^{-1}) is in excellent agreement with the m.a.d. we measured for our radial velocity standards.

We checked that the ΔV_r distribution of our binaries is indeed distinct from physically unassociated stars. We used the Galactic model from Paper I that gives the expected three-dimensional velocity distribution for any position in the Galaxy or, if desired, a randomly chosen velocity from that distribution. We compared with a sample that has been selected in a similar manner to the pairs in our observed sample. Hence, at the Galactic positions of each of the observed pairs, we generated pairs of three-dimensional velocities until a pair with matching proper motions was found. The proper motion matching criterion was the same as that in Paper I. For statistical robustness, we conducted 10^6 realizations of this simulation; the normalized histogram of the resultant distribution is shown with dotted lines in the right panel of Figure 4. For a quantitative assessment of the difference between the simulated and observed ΔV_r distributions, we performed the Kolmogorov–Smirnov test (Press et al. 1992) and found a 0.93% probability that the two were drawn from the same parent population. We conclude that the ΔV_r distribution of our observed binaries is much narrower than the scatter expected of two unassociated stars.

Thirteen (12.6%) of the pairs have V_r that disagree at $>3\sigma$. The SLoWPoKES catalog only contains pairs with a probability of chance alignment, P_f, less than 5%, meaning fewer than 5 of 103 pairs were expected to be false positives. In fact, P_f was tabulated for each pair in Paper I; the cumulative sum of chance alignments was only 0.3%, implying that <1 pair was expected to be false positives. As shown in the left panel of Figure 5, there is no trend in ΔV_r as a function of P_f. There are discrepant pairs at all values of P_f. However, as can be seen in the right panel of Figure 5, there is a significant trend of ΔV_r with the S/N in the spectra. The pairs with the largest ΔV_r values are at low S/N, while there are no discrepant pairs at high S/N. This suggests that the cross-correlation process and the measurements of V_r might have been adversely affected by the noise, yielding noisier radial velocities. In addition, given the large higher-order multiplicity fraction seen in SLoWPoKES (45%; Law et al. 2010), the presence of more SBs in our observed sample cannot be ruled out by our low-resolution spectra.

In summary, the vast majority of the sample pairs show agreement in their radial velocities, as expected for physical
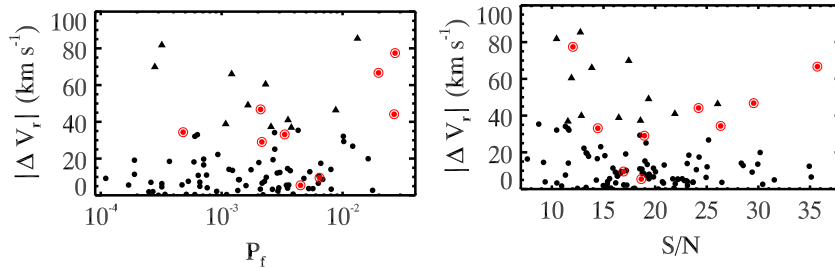
Figure 5. Left: the probability of chance alignment (P_f) calculated using the Galactic model by Paper I vs. the difference in radial velocity between components for the 113 SLoWPoKES CPM pairs observed in this program. Right: systems with a lower S/N (red) have a higher dispersion in ΔV_r, suggesting that the observed discrepancy might be due to the lower S/N. Candidate SBs are shown as red, concentric circles while pairs with $\Delta V_r > 3\sigma$ are shown as triangles.

(A color version of this figure is available in the online journal.)
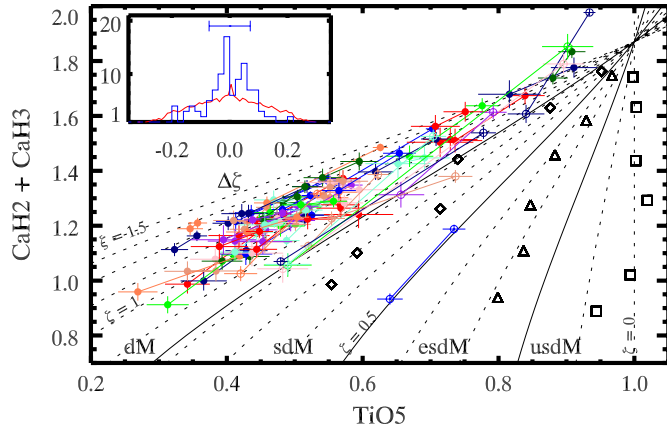
Figure 6. Distribution of the observed M dwarf binaries, with components of a system connected by solid lines, in the CaH/TiO space confirms the iso-ζ contours with $\zeta = 0.0, 0.1, 0.2, ..., 1.5$ (dotted lines), albeit with some deviation at the highest values (toward top right). The distribution of $\Delta\zeta$ (blue histogram; inset) peaks at ~ 0 and is significantly different from a distribution for two randomly paired dMs (red solid line). However, the scatter in $\Delta\zeta$ is large; the bar at the middle-top of the inset shows the scatter in the error of $\Delta\zeta$ ($\sigma_{\Delta\zeta}$). The solid contours demarcate the boundary between the dM/sdM/esdM/usdM classes while the K7–M5 spectral standards for the sdM (diamonds), esdM (triangles), and usdM (squares) classes are shown (LRS07). Early-type M stars are at the upper right, late types at the lower left.

(A color version of this figure is available in the online journal.)

binaries. Pairs with discrepant V_r values have spectra with low observed S/N or are (candidate) hierarchical systems with an SB.

3.3. Metallicity Index Calibration

Figure 6 shows the observed SLoWPoKES pairs, with the components of each pair connected with a solid line, in the CaH–TiO space with the dotted lines showing the iso-ζ lines from LRS07 for $\zeta = 0.1$–1.5 in steps of 0.1. The solid lines delineate the boundary between the dM/sdM/esdM/usdM classes ($\zeta = 0.825, 0.500,$ and 0.200, respectively); the single-star spectral standards for the sdM (diamonds), esdM (triangles), and usdM (squares) classes are also shown (LRS07). For clarity, only pairs whose error bars, in both CaH and TiO5 of both pairs, are smaller than the median error are plotted. Most of the observed pairs are dMs, i.e., part of the thin disk with roughly solar metallicity. This is not surprising for a bright sample located within $\sim$200–300 pc of the Sun as the local neighborhood is largely dominated by thin-disk stars (Bochanski et al. 2010).

Most of the binary pairs lie parallel to the iso-ζ lines, within the error bars. The inset in Figure 6 shows the distribution of

$\Delta\zeta$, which is centered around zero but has substantial scatter. Quantitatively, the median and m.a.d. are -0.005 and 0.066, respectively, indicating that for the vast majority of the observed pairs, ζ correctly infers a common metallicity for the two stars in each pair.

To test whether the observed $\Delta\zeta$ distribution was merely the intrinsic scatter in $\Delta\zeta$, we randomly selected 113 pairs of disk stars ($\zeta = 0.825$–1.100) in the similar brightness range as the SLoWPoKES sample ($r < 20$) and with high proper motions ($\mu \geqslant 40$ mas yr^{-1}) from the SDSS spectroscopic catalog (West et al. 2011) and calculated the $\Delta\zeta$ distribution. There were 8030 stars in the DR7 spectroscopic sample that met these criteria; 113 pairs were randomly selected from this sample and their $\Delta\zeta$ distribution calculated. We performed this simulation 10^5 times; the resultant distribution is plotted in red in the inset of Figure 6. The simulated $\Delta\zeta$ distribution is less centrally peaked, and much broader, compared with our observed distribution. The Kolmogorov–Smirnov test (Press et al. 1992) finds a probability of 3.3×10^{-25} that the two distributions were drawn from the same parent population. We conclude that the metallicities of components of SLoWPoKES binaries observed in this program are more similar to each other than those of two randomly paired thin-disk stars. As components of a binary system are expected to have formed of the same material, this further serves to confirm the physical association of the pairs. Furthermore, it strengthens the argument that ζ is a reliable proxy for relative metallicity.

However, Figure 6 also demonstrates some deficiencies in the definition of ζ. First, $\Delta\zeta$ is more than 3 m.a.d. away from zero for $\sim$18% of the pairs versus the $\sim$5% expected for a normal distribution. They are discrepant especially at large values of TiO5 and CaH2 + CaH3, i.e., for higher-mass M dwarfs, perhaps suggesting a break in the ζ(TiO5, CaH2 + CaH3) relation. Large errors in this regime further complicate the issue, as the discrepant ζ values could result from the difficulty of measuring the shallower TiO5, CaH2, and CaH3 band heads in late-K and early-M dwarfs. It is also evident how the iso-ζ contours converge at the higher masses as pointed out by LRS07. On the other hand, the discrepancy persists for the higher-mass pairs with smaller error bars, as can be clearly seen in Figure 6. Second, and perhaps more importantly, our measured ζ values increase and become supersolar (i.e., $\zeta > 1$) for the higher-mass stars. This is inconsistent with the expectation: given the apparent magnitude constraints ($r \sim 15$–17), the higher-mass stars in this sample can be expected to be farther away and, hence, at larger Galactic heights given that most of the SDSS sight lines are at high Galactic latitudes (Ivezić et al. 2008). Stars at high latitudes are, on average, older; consequently, if anything, they might be expected to have lower metallicities

Table 4
Coefficients, a_N, for Equation (2)

Coefficients	LRS07	This Study
a_0	−0.050	−0.047
a_1	−0.118	−0.127
a_2	+0.670	+0.694
a_3	−0.164	−0.183
a_4	. . .	−0.005

(West et al. 2008). Yet, the ζ-index yields the opposite. This result necessitates a redefinition of ζ. With a spectroscopic sample of 113 visually resolved binaries, we are in a unique position to modify the definition of ζ.

Given the lack of subdwarf pairs in our sample, any recalibration of ζ would be systematically biased to high metallicity. Hence, we conducted a search for companions around the subdwarfs ($\zeta < 0.825$) in the SDSS DR7 spectroscopic catalog (West et al. 2011) with extant SDSS spectra. We have identified a sample of 10 pairs with low values of ζ, shown as open circles in Figure 6. The full sample that was identified in the search will be presented in a future paper (S. Dhital et al. 2012, in preparation). One of the added pairs is at the sdM/esdM boundary, while the other nine are at the dM/sdM boundary. While small, this sample provides an invaluable constraint in the low-metallicity regime.

LRS07 defined ζ as

$$\zeta = \frac{1 - \text{TiO5}}{1 - [\text{TiO5}]_{Z_\odot}}, \qquad (1)$$

where $[\text{TiO5}]_{Z_\odot}$ is a third-order polynomial of (CaH2+CaH3)

$$[\text{TiO5}]_{Z_\odot} = \sum_N a_N (\text{CaH2} + \text{CaH3})^N, \qquad (2)$$

and where the coefficients, a_N, are tabulated in Table 4 and were obtained as a single fit to the TiO5 index as a function of the CaH2+CaH3 index for a kinematically selected sample of thin-disk stars.

We can recalibrate ζ by varying the functional form of $[\text{TiO5}]_{Z_\odot}$ in Equation (2) such that the scatter in the $\Delta\zeta$ distribution is minimized and distributed around zero. As noted earlier, the LRS07 definition, to first order, is a robust measure of relative metallicity, and any recalibration need only be a small perturbation about the LRS07 definition. Moreover, as the definition was based on the distribution of (TiO5, CaH2+CaH3) of disk stars, it is a good starting point for the recalibration. So we only chose to explore the coefficient values within ±0.03 of the LRS07 values in steps of $\Delta = 0.001$. We have introduced a fourth-order term in Equation (2), with an initial guess of zero, based on the observed deviation of higher-mass pairs from the iso-ζ lines. The best-fit values for the coefficients were found by minimizing χ^2, where $\Delta\zeta = 0$ was assumed to be the model. All dM/sdM pairs, except for the ones with the large error bars, were considered for the fit.

Figure 7 shows the new iso-ζ contours, with the coefficients tabulated in Table 4. The contours look significantly different despite small changes in the coefficients, reflecting the very sensitive dependence of ζ on its independent variables. The differences can be summarized as follows:

1. The scatter in the $\Delta\zeta$ is smaller, with the m.a.d. decreasing from 0.060 to 0.044. There are fewer outliers as well, with
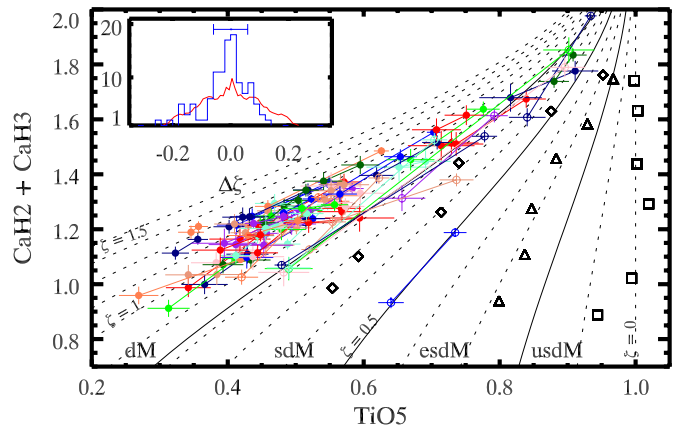

Figure 7. Same as Figure 6 but with the redefined ζ, which was done by adding a fourth-order term in Equation (2) and refitting the coefficients by perturbing about the LRS07 values. The new definition of ζ minimizes the scatter in the $\Delta\zeta$ distribution and yields lower metallicity for stars at larger Galactic heights, which are expected to be older and have a lower metallicity. The $\Delta\zeta$ distribution is now also much more centrally peaked as compared with random pairings of unassociated stars (compare to the inset of Figure 6).

(A color version of this figure is available in the online journal.)

the values converging toward $\Delta\zeta = 0$. As the median error in $\Delta\zeta$ is bigger than the scatter in $\Delta\zeta$, decreasing the scatter further is not possible unless higher-S/N data are obtained. The $\Delta\zeta$ distribution is much more centrally peaked as compared with randomly paired field stars.

2. With only a few pairs at the higher masses (large TiO5), ζ yields more consistent values between components of the higher-mass dMs than in the original LRS07 definition. This congruence is important if we are to have the same metallicity proxy for all low-mass stars and is likely to improve as more pairs are added to that locus. It is especially reassuring to get the same value of ζ for the components of pairs with large differences in mass, CaH2+CaH3, and TiO5; the ζ values calculated from the previous definition were especially discrepant as the primary was assigned an artificially super-solar ζ. With the new definition, the higher-mass dMs instead have slightly sub-solar ζ, which is what is expected for stars at larger Galactic heights.

3. The new iso-ζ contours are less crowded at the higher-mass regime, allowing for a more robust determination of metallicity. In fact, the iso-ζ do not converge before (TiO5, CaH2+CaH3) = (1,2), hence expanding the regime for sdMs/esdMs/usdMs. The metallicity classes also become more sensitive to TiO5 relative to CaH2+CaH3. However, with the new contours for ζ, the previously defined standards for the metallicity classes are assessed to be more metal-poor and are no longer in the same class. While this argues for a definition of new standards, we advise against such a revision until there are more subdwarf binaries to more robustly calibrate the contours in that regime.

In general, the new definition of ζ better fits the observed sample of visual binaries, as well as resolving outstanding issues at the high-mass end. However, owing to a paucity of subdwarf pairs, it leaves the low-metallicity regime rather unconstrained. ζ looks to be a good proxy for metallicity, and future observations of subdwarf pairs should calibrate it for all low-mass stars. Studies that are using subdwarf binaries (S. Dhital et al. 2012, in preparation) and F/G–K/M binaries (J. J. Bochanski et al. 2012, in preparation; S. Lépine et al. 2012, in

preparation) are already underway and are part of a larger effort to measure the absolute metallicity of low-mass stars.

3.4. Hα Activity

As M dwarf photospheres are too cold to excite electrons into the $n = 2$ level, any observed Hα feature, either in absorption or in emission, is chromospheric in origin. The weakest chromospheres will exhibit no Hα; as the activity levels increase, Hα will be observed in absorption with the line filling in and eventually going into emission for the most active M dwarfs (Stauffer & Hartmann 1986; Cram & Giampapa 1987; Walkowicz & Hawley 2009). As Hα is in absorption for both inactive and moderately active M dwarfs, Hα emission has traditionally been used as the tracer of chromospheric activity and is biased toward the most active M dwarfs (e.g., West et al. 2011).

In our sample, 11 of the 113 pairs showed clear evidence of Hα emission in both components, while 3 pairs had only one component with Hα in emission. In addition, 33 pairs showed Hα absorption in both components and 22 pairs in one component; the remaining 47 were classified as inactive. The large fraction (39%) of stars with Hα absorption is in accordance with the nearby M dwarfs in the Palomar/MSU Nearby Star Spectroscopic Survey (Gizis et al. 2002). Overall, for 91 of the 113 (81%) pairs in our sample, both components of a pair showed similar levels of activity—in emission, absorption, or the lack of activity. For the pairs with both components having Hα emission, we converted the equivalent width in Hα to $L_{Hα}/L_{bol}$—the ratio of the Hα luminosity to the bolometric luminosity that is independent of spectral type—following Walkowicz et al. (2004) and West et al. (2004); all pairs had comparable levels of $L_{Hα}/L_{bol}$ within the error bars except for the two where the active primary was identified as a candidate SB and had an inactive secondary. The tidal forces due to the tight companion have presumably enhanced the activity of the primary (Shkolnik et al. 2010; Silvestri et al. 2006).

As Hα activity depends strongly on mass (West et al. 2008), one way to compare the intrinsic variability in activity levels is by only looking at pairs with components of similar masses. All sixteen pairs with Hα in emission or absorption in both components and with similar colors ($\Delta(r - z) < 0.2$) had Hα equivalent widths within 130% of each other. Compared with the 200%–300% difference in Hα activity exhibited by M dwarfs over time (Bell et al. 2011), the components of the similar-mass binary pairs in our sample exhibit a much smaller difference in Hα activity. This is consistent with the expectation that stars of similar ages and masses have comparable activity levels, presumably because they experience similar spin-down rates.

4. CONCLUSIONS

We have carried out a spectroscopic follow-up study of 113 ultra-wide, low-mass CPM binary systems from the SLoWPoKES catalog (Paper I) using the GOLDCAM spectrograph on the KPNO 2.1 m telescope. We measured the radial velocities of each component by cross-correlating them with appropriate standards and used them to assess the fidelity of pairs in the SLoWPoKES catalog. Ninety-five of the 113 (84%) pairs have the same radial velocity within 3σ. At least five of the pairs with discrepant radial velocities are candidate SBs, which would explain the difference. There may be additional spectroscopic companions undetected in our low-resolution spectra. Law et al. (2010) found that 45% of the SLoWPoKES systems are either

hierarchical triples or quadruples. Either high-resolution spectroscopy or imaging would be needed to identify the close companions and to further quantify the incidence of higher-order systems in wide binaries.

We examined the Hα activity in our observed sample. The components of binary pairs exhibited overwhelmingly comparable levels of Hα activity. Moreover, the ΔHα of the pairs with similar $r - z$ colors and two active components, while large, was several times smaller than the variation seen in single M dwarfs. Our results corroborate that low-mass stars of the same mass should spin down at similar rates over time. However, larger samples of active stars are needed to confirm this finding and to constrain the rate of this spin-down.

We tested the LRS07 ζ-index and found that, to first order, it is a robust measure of relative metallicity. The value of ζ for the two components in each binary system matches within the error bars for most pairs, indicating a common metallicity as expected. However, we find a systematic bias for the higher-mass M dwarfs such that ζ overestimates the metallicity. Assuming that all of the pairs are physically associated systems and have the same metallicity, we have redefined ζ. While the shift is small, it better represents iso-metallicity lines in the high-metallicity regime and represents an incremental step toward defining an absolute metallicity scale for low-mass dwarfs. Planned further observations should extend the calibration of ζ and map it to an absolute metallicity scale in the near future.

REFERENCES

Abazajian, K. N., Adelman-McCarthy, J. K., Agüeros, M. A., et al. 2009, ApJS, 182, 543
Barnes, S. A. 2003, ApJ, 586, 464
Barnes, S. A. 2007, ApJ, 669, 1167
Bate, M. R., Bonnell, I. A., & Bromm, V. 2002, MNRAS, 336, 705
Bell, K. J., Hilton, E. J., Davenport, J. R. A., et al. 2011, arXiv:1112.1411B
Bessell, M. S. 1982, PASA, 4, 417
Bochanski, J. J., Hawley, S. L., Covey, K. R., et al. 2010, AJ, 139, 2679
Bochanski, J. J., Munn, J. A., Hawley, S. L., et al. 2007a, AJ, 134, 2418
Bochanski, J. J., West, A. A., Hawley, S. L., & Covey, K. R. 2007b, AJ, 133, 531
Bonfils, X., Delfosse, X., Udry, S., et al. 2005, A&A, 442, 635
Burgasser, A. J., & Kirkpatrick, J. D. 2006, ApJ, 645, 1485
Burgasser, A. J., Kirkpatrick, J. D., & Lowrance, P. J. 2005, AJ, 129, 2849
Connelley, M. S., Reipurth, B., & Tokunaga, A. T. 2009, AJ, 138, 1193
Covey, K. R., Hawley, S. L., Bochanski, J. J., et al. 2008, AJ, 136, 1778
Covey, K. R., Ivezić, Ž., Schlegel, D., et al. 2007, AJ, 134, 2398
Cram, L. E., & Giampapa, M. S. 1987, ApJ, 323, 316
Delfosse, X., Forveille, T., Perrier, C., & Mayor, M. 1998, A&A, 331, 581
Delorme, P., Collier Cameron, A., Hebb, L., et al. 2010, in SF2A-2010: Proc. Annual Meeting of the French Society of Astronomy and Astrophysics, ed. S. Boissier, M. Heydari-Malayeri, R. Samadi, & D. Valls-Gabaud, 243
Dhital, S., West, A. A., Stassun, K. G., & Bochanski, J. J. 2010, AJ, 139, 2566
Faherty, J. K., Burgasser, A. J., West, A. A., et al. 2010, AJ, 139, 176
Fuchs, B., Dettbarn, C., Rix, H.-W., et al. 2009, AJ, 137, 4149
Gizis, J. E. 1997, AJ, 113, 806
Gizis, J. E., Reid, I. N., & Hawley, S. L. 2002, AJ, 123, 3356
Hauschildt, P. H., Allard, F., & Baron, E. 1999, ApJ, 512, 377
Hilton, E. J., West, A. A., Hawley, S. L., & Kowalski, A. F. 2010, AJ, 140, 1402
Ivezić, Ž., Sesar, B., Jurić, M., et al. 2008, ApJ, 684, 287
Johnson, J. A., & Apps, K. 2009, ApJ, 699, 933
Jurić, M., Ivezić, Ž., Brooks, A., et al. 2008, ApJ, 673, 864
Kirkpatrick, J. D., Henry, T. J., & McCarthy, D. W., Jr. 1991, ApJS, 77, 417
Kowalski, A. F., Hawley, S. L., Hilton, E. J., et al. 2009, AJ, 138, 633
Kraus, A. L., & Hillenbrand, L. A. 2007, AJ, 134, 2340

Kruse, E. A., Berger, E., Knapp, G. R., et al. 2010, ApJ, 722, 1352
Law, N. M., Dhital, S., Kraus, A., Stassun, K. G., & West, A. A. 2010, ApJ, 720, 1727
Laws, C., Gonzalez, G., Walker, K. M., et al. 2003, AJ, 125, 2664
Lépine, S., Rich, R. M., & Shara, M. M. 2003, AJ, 125, 1598
Lépine, S., Rich, R. M., & Shara, M. M. 2007, ApJ, 669, 1235
López-Morales, M. 2007, ApJ, 660, 732
Massey, P., Valdes, F., & Barnes, J. 1992, http://iraf.net/faqman/index.php?op=view&t=20
Matijevič, G., Zwitter, T., Munari, U., et al. 2010, AJ, 140, 184
Mohanty, S., & Basri, G. 2003, ApJ, 583, 451
Press, W. H., Teukolsky, S. A., Vetterling, W. T., & Flannery, B. P. 1992, Numerical Recipes in FORTRAN: The Art of Scientific Computing (2nd ed.; Cambridge: Cambridge Univ. Press)
Reid, I. N., Hawley, S. L., & Gizis, J. E. 1995, AJ, 110, 1838
Rojas-Ayala, B., Covey, K. R., Muirhead, P. S., & Lloyd, J. P. 2010, ApJ, 720, L113
Schlaufman, K. C., & Laughlin, G. 2010, A&A, 519, A105
Shkolnik, E. L., Hebb, L., Liu, M. C., Reid, I. N., & Cameron, A. C. 2010, ApJ, 716, 1522
Silvestri, N. M., Hawley, S. L., West, A. A., et al. 2006, AJ, 131, 1674
Skrutskie, M. F., Cutri, R. M., Stiening, R., et al. 2006, AJ, 131, 1163
Skumanich, A. 1972, ApJ, 171, 565
Stauffer, J. R., & Hartmann, L. W. 1986, ApJS, 61, 531
Tokovinin, A. A. 1997, Astron. Lett., 23, 727
Valenti, J. A., & Fischer, D. A. 2008, Phys. Scr. T, 130, 014003
Walkowicz, L. M., & Hawley, S. L. 2009, AJ, 137, 3297
Walkowicz, L. M., Hawley, S. L., & West, A. A. 2004, PASP, 116, 1105
West, A. A., & Basri, G. 2009, ApJ, 693, 1283
West, A. A., Bochanski, J. J., Hawley, S. L., et al. 2006, AJ, 132, 2507
West, A. A., Hawley, S. L., Bochanski, J. J., et al. 2008, AJ, 135, 785
West, A. A., Hawley, S. L., Walkowicz, L. M., et al. 2004, AJ, 128, 426
West, A. A., Morgan, D. P., Bochanski, J. J., et al. 2011, AJ, 141, 97
Witte, S., Helling, C., Barman, T., Heidrich, N., & Hauschildt, P. H. 2011, A&A, 529, A44
Woolf, V. M., Lépine, S., & Wallerstein, G. 2009, PASP, 121, 117
York, D. G., Adelman, J., Anderson, J. E., Jr., et al. 2000, AJ, 120, 1579